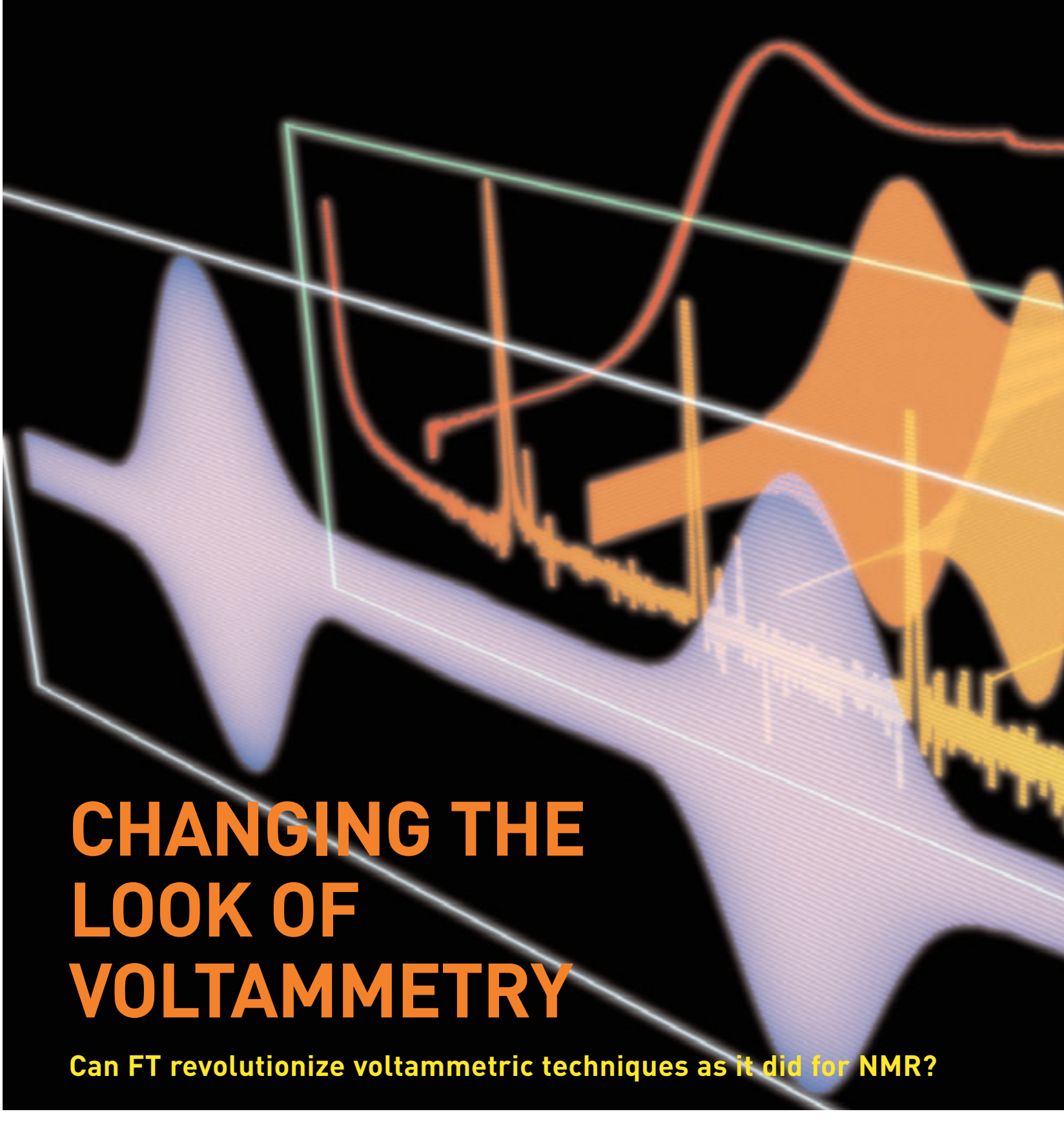

CHANGING THE LOOK OF VOLTAMMETRY

Can FT revolutionize voltammetric techniques as it did for NMR?

The linear, staircase, and cyclic modes of dc voltammetry have become the electrochemical methods of choice for rapidly gaining insights into the mechanistic details of the electron-transfer processes that are significant in chemistry, biology, physics, industrial chemistry, and other disciplines (*1*–*4*). In this article, we will show how a variety of voltammetric techniques that are often considered quite unlike really differ only in the combination of sine waves superimposed onto a dc potential. Because of this characteristic, instrumentation and simulations only need the capacity to generate a dc ramp and sine waves of any combination of frequencies and amplitudes. Also, the data obtained in the time domain can be transformed into the frequency domain to achieve a major level of unification in voltammetric methods. In this integrated approach, differences in techniques are now represented by mechanism-dependent patterns of behavior detected at fre-

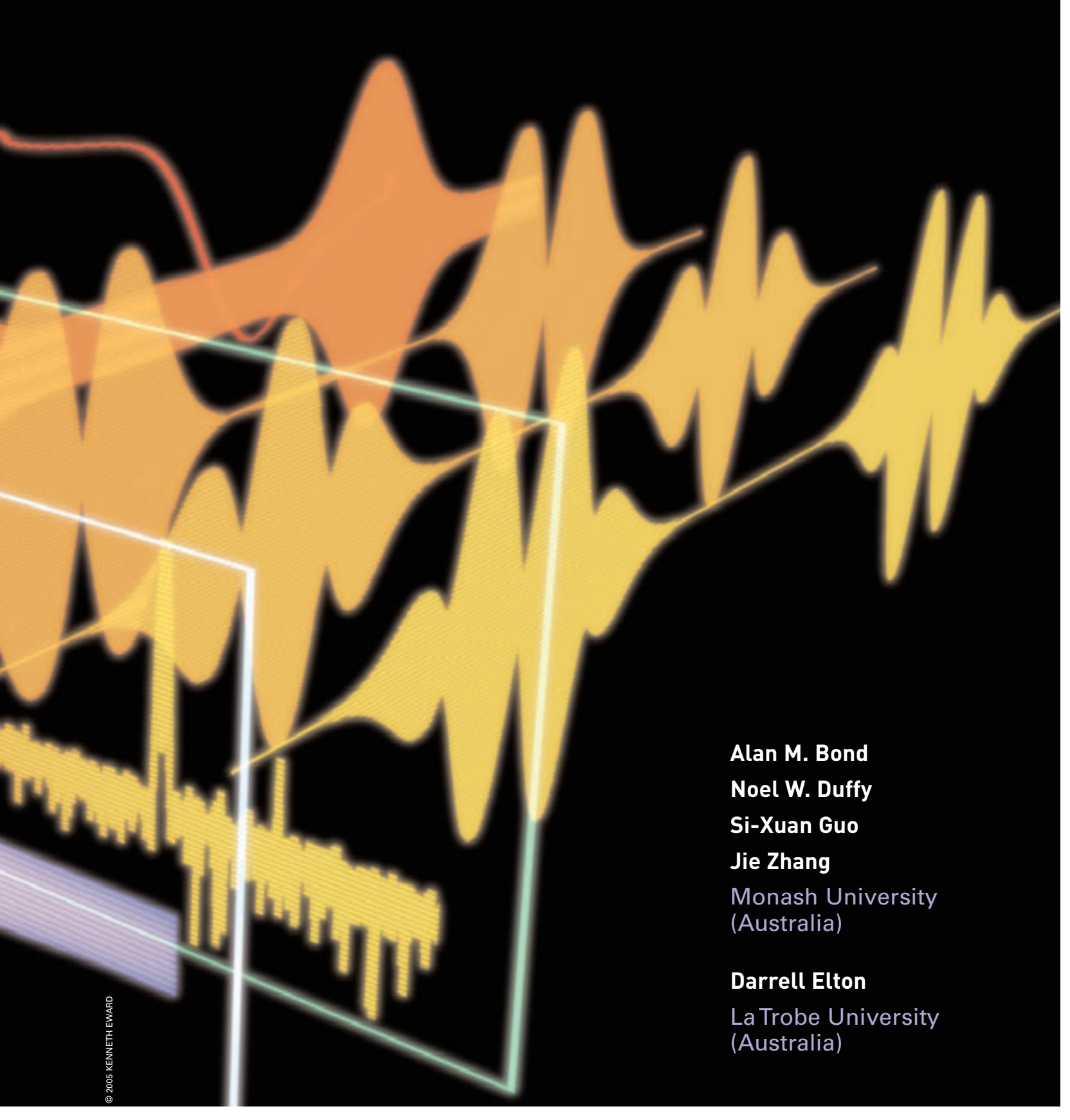

Alan M. Bond
Noel W. Duffy
Si-Xuan Guo
Jie Zhang
Monash University (Australia)

Darrell Elton
La Trobe University (Australia)

quencies that are related to the input signal. Thus, differences are no longer related to the use of small- or large-amplitude considerations, and nonlinearity—often regarded as a complicating factor—is now seen as a distinct advantage.

Traditional techniques

In voltammetry, a time t dependent dc potential E_{dc} (whose value relative to a reference electrode is known) is applied to a working electrode that is in contact with an electroactive species. In cyclic voltammetry (CV; Figure 1a), the potential is commonly cycled by scanning in one direction until the so-called switching potential is reached and then reversing the scan. This approach provides information about both the oxidation and reduction components of an electron-transfer process. Measurement of the current I as a function of E_{dc} generates a voltammogram (Figures 1b–d). An equivalent plot of I versus t

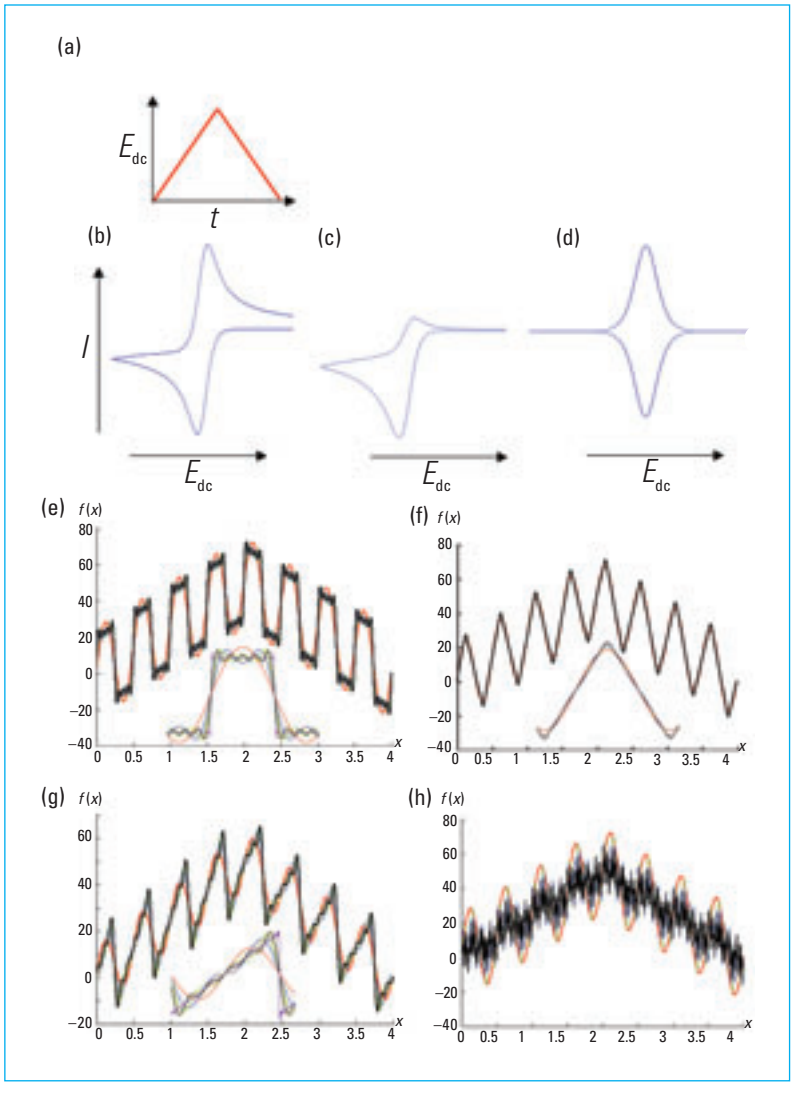

FIGURE 1. Waves and waves.

(a) Typical waveform used in dc CV. Typical dc voltammograms obtained for (b) reversible reaction, (c) coupled chemical reaction, and (d) surface-confined classes of electron transfer. Fourier series approximations; displayed are the 1st (red) to the 5th (black) and the 100th (purple) summed terms of the expansion for (e) square-wave, (f) triangle, and (g) sawtooth waveforms; (h) a waveform made up of 8 nonharmonically related sine components.

can also be constructed because E_{dc} is a function of t. For example, $E_{dc} = E_{initial} + \nu t$ applies in linear sweep voltammetry, in which $E_{initial}$ is the initial potential and ν is the scan rate.

Acquiring the relevant E–I–t data is one challenge faced by those who wish to understand all aspects of an electron-transfer reaction taking place at an electrode–solution (electrolyte) interface. The companion challenge is to interpret the E–I–t information in terms of each of the faradaic (e.g., electron-transfer) and nonfaradaic (e.g., double-layer capacitance, uncompensated resistance) terms that contribute to the experimental data. In practice, mechanistic understanding of the nuances of an electrode process initially requires qualitative recognition and then quantitative modeling of the time- and concentration-dependent patterns of behavior that emerge from examining the voltammetric data. Ultimately, it should be possible to describe the peak potential, peak current, and wave shape that are derived from a combination of the faradaic and underlying background or nonfaradaic components by a mathematical model that mimics the time (νt) dependence of the experimental data.

Different patterns of behavior are detected when dc CV is performed on the reversible reduction of dissolved reactant A to dissolved product B (Figure 1b, Equation 1) followed by its conversion to give dissolved C (Figure 1c, Equations 1 and 2) and when the surface-confined A and B undergo an electron-transfer process (Figure 1d, Equation 3). Ideally, each mechanism would produce its own characteristic scan-rate-dependent E–I–t response, but in practice not all mechanisms will be experimentally distinguishable.

$$A_{solution} + e^- \rightleftharpoons B_{solution} \quad (1)$$

$$B_{solution} \rightarrow C_{solution} \quad (2)$$

$$A_{surface\text{-}confined} + e^- \rightleftharpoons B_{surface\text{-}confined} \quad (3)$$

Before any realistic theory versus experimental comparisons can be undertaken, contributions from background current and uncompensated resistance R_u must be included in the theoretically predicted voltammogram. Alternatively, it may be possible to remove the nonfaradaic contributions to the experimental data; the modified voltammograms can then be compared with those obtained solely on the basis of the inherently simpler theory applicable to the faradaic component.

Direct global comparison of experimental and simulated data is a daunting undertaking because so many parameters contribute to the E–I–t data. One valuable trick is to analyze the data in a series of selected regions of potential that are highly sensitive to just one or two of the parameters and relatively insensitive to all the others. Only at the conclusion of this process is the global comparison of experimental and simulated data undertaken. In principle, an infinite number of mechanisms are available, so achieving a unique solution can never be guaranteed. To enhance the probability of obtaining the "correct" mechanism, examining the voltammetric response under a sufficiently wide range of conditions is mandatory. Furthermore, independent evaluation of any thermodynamic, kinetic, or electrochemical parameters required to interpret the voltammetric data should be undertaken as a quality-control measure. In some circumstances, these independently obtained parameters would be included in the simulation as known, rather than unknown, parameters (e.g., electrode area, diffusion coefficient, resistance, reactant concentration, temperature).

FT voltammetry

Any strategy that enhances the quality and/or quantity of voltammetric data obtained per experiment, enables faradaic and

nonfaradaic terms to be separated, or enhances discrimination of closely related mechanisms is highly advantageous. To more easily elucidate the electrode mechanism, numerous techniques have been proposed in which a periodic signal is superimposed onto the dc waveform (Figure 1e–h). Examples include ac, square-wave, and pulse voltammetry and impedance spectroscopy. They are often portrayed as distinct techniques with their own individual characteristics (*1–10*). This traditional form of classification arose because each approach was described at a different time in history, each with its own instrumentation, theory, data analysis, and applications; therefore, the impression is that a vast arsenal of fundamentally different techniques are available to supplement the dc form of voltammetry.

Because of this tradition, ac voltammetry and impedance spectroscopy are usually described in terms of small-amplitude sinusoidal perturbations and used in mechanistic studies. Conversely, Barker square-wave, Osteryoung square-wave, and differential-pulse forms of voltammetry are commonly described in terms of large-amplitude perturbations and are often used in analytical applications because they are believed to have superior faradaic-to-nonfaradaic-current ratios (*7*). However, there is no inherent reason not to use large-amplitude sinusoidal methods in analytical applications or small-amplitude square-wave or pulse methods in fundamental studies.

In fact, if the relevant periodic waveform is thought of as a sum of sine waves represented by the Fourier series (*11*), then it becomes very obvious that the only difference among these techniques is the combination of sine waves used as the "input"; therefore, treating each voltammetric technique in isolation makes no sense. Likewise, for each technique, the frequency-domain "output" only differs in a mechanism-dependent manner with respect to the patterns of behavior that each sine-wave combination produces. These characteristic patterns are easily recognized after an FT–inverse FT sequence is used and the data are displayed as harmonic or component contributions (Figures 2c–e). This process emphasizes the similarities and differences of each method in a more intuitively obvious manner than the traditional time-domain forms of output presentation.

To illustrate the principles of FT voltammetry, the Fourier series sine-wave combination of the four periodic waveforms (Figures 1e–h) must be considered in more detail. If a single sine wave of amplitude ΔE and frequency ω is superimposed onto E_{dc} as in ac voltammetry, then $E_t = E_{dc} + \Delta E \sin(\omega t)$. By comparison, the waveform (Figure 1e) applied in square-wave

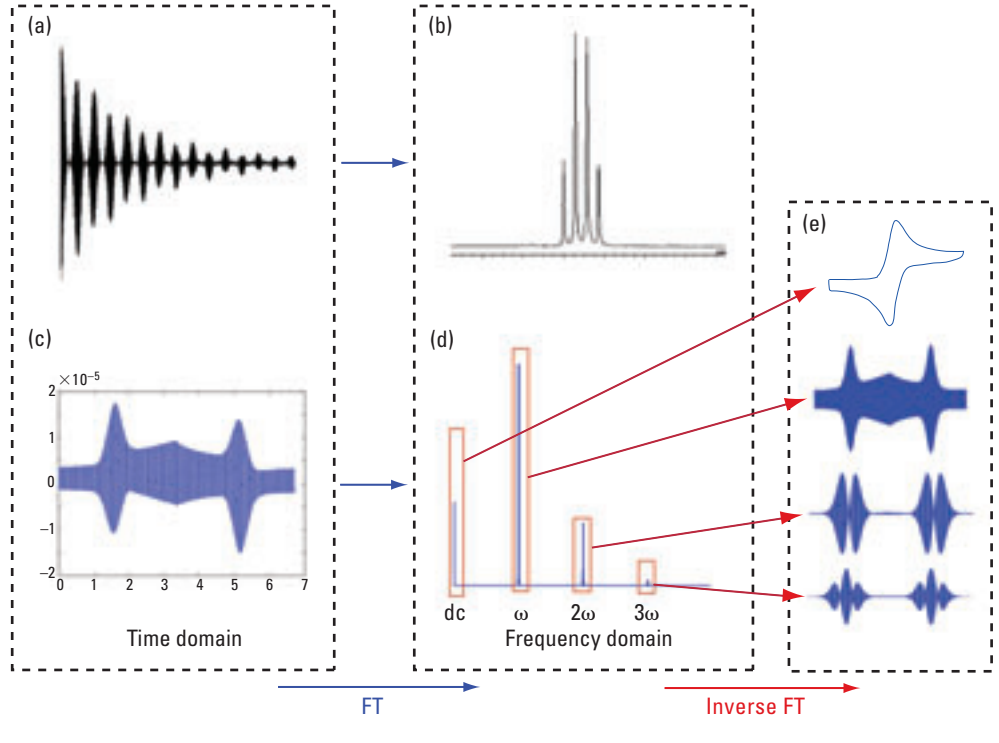

FIGURE 2. Transformers.

(a) Time and (b) frequency representations of ^{1}H FT-NMR data obtained from CH_3CHO. (c) Time and (d) frequency representations of single-sine-wave FT voltammetric data for the oxidation of ferrocene in dichloromethane at a platinum electrode. (e) Separated dc and ac components represented in the time domain.

voltammetry would be represented by the expression

$$E_t = E_{dc} + \frac{4\Delta E}{\pi} \sum_{n=1,3,5\ldots}^{k} \frac{1}{n} \sin(n\omega t) \quad (4)$$

Analogously, a voltammetric technique developed from application of a triangular waveform (Figure 1f) would be represented by

$$E_t = E_{dc} + \frac{8\Delta E}{\pi^2} \sum_{n=1,3,5\ldots}^{k} \frac{(-1)^{(n-1)/2}}{n^2} \sin(n\omega t) \quad (5)$$

In the case of a sawtooth voltammetric waveform (Figure 1g), the representation in terms of a sine-wave series is

$$E_t = E_{dc} + \frac{2\Delta E}{\pi} \sum_{n=1,2,3\ldots}^{k} \frac{(-1)^n}{n} \sin(n\omega t) \quad (6)$$

Finally, if N sine waves of selected ω (ω_1, ω_2, . . ., ω_N) and ΔE (ΔE_1, ΔE_2, . . ., ΔE_N) are combined (Figure 1h), then

$$E_t = E_{dc} + \sum_{n=1,2,3\ldots}^{N} \Delta E_n \sin(\omega_n t) \quad (7)$$

In the most commonly used form of impedance spectroscopy, many small-amplitude, phase-randomized sine waves are superimposed onto a constant dc potential (*5*). Thus, in this article, impedance spectroscopy is simply another variation of FT voltammetry.

In the ideal Fourier representation, $k = \infty$ in the square, triangular, sawtooth (Equations 4–6, respectively), and other related waveforms. Use of a waveform with $k \geq 35$ has been generally shown to provide results that are experimentally indistinguishable from those obtained with the pure waveform ($k = \infty$) for these nonsinusoidal cases; however, for a triangular waveform, k can be significantly <35 and the desired result can still be achieved.

In principle, an electrochemical cell represents a nonlinear response system with respect to the faradaic component. Consequently, superimposition of a sine wave of a certain ω onto a dc potential (where oxidation or reduction occurs) will generate a response that contains a dc contribution and fundamental (at ω), second (at 2ω), and higher harmonic contributions. In contrast, an 8-sine combination waveform (Figure 1h) will produce a response that contains a dc term; 8 fundamental harmonic components at ω_1, . . ., ω_8; numerous second- and higher-harmonic terms derived from each component; and contributions at the frequency sums ($\omega_1 + \omega_2$, $\omega_1 + \omega_3$, . . .) and frequency differences ($\omega_8 - \omega_1$, $\omega_8 - \omega_2$, . . .). The square-wave response in terms of a sine-wave representation constitutes a waveform that will generate a dc term and an infinite number of components at all odd multiples of the fundamental frequency (ω, 3ω, 5ω, . . .). In this case, a direct relationship exists between the odd components applied and the harmonics detected, but responses at 2ω, 4ω, 6ω, . . . can emerge from the nonlinearity.

A variety of unlike voltammetric techniques really differ only in the combination of sine waves superimposed onto a dc potential.

In impedance spectroscopy, small-amplitude perturbations and other procedures such as phase randomization are used in an attempt to minimize second- and higher-order terms so that modeling can be linearized (*5*). However, this may be unwise because second-order terms are exceptionally information-rich and exhibit readily recognized patterns of behavior that are extremely valuable in electrode mechanism evaluation. All of these terms may provide vastly superior faradaic-to-background-current ratios (*12*). Granted, the additional complexity introduced by the second-order terms means that the response must be simulated; analytical mathematical solutions that are commonly available with linearized systems may not be available. But nowadays, the same desktop computer that controls the experiment is sufficiently fast to undertake the required simulations.

The double-layer component of the voltammetric background signal has traditionally been represented as a linear response system. In this ideal situation, the double-layer charging current C_{dl} in a Fourier-transformed output therefore will only be present in the dc term for all waveforms and at ωt for the single-sine-wave case; at ω_1, . . ., ω_8 for an 8-component system; at ω, 3ω, 5ω, . . . for the square-wave case; and at all applied frequencies in impedance spectroscopy. It therefore follows for the sine-wave case that C_{dl}-based components will be absent at the second and higher harmonics. It now becomes obvious how differing patterns of behavior of faradaic and nonfaradaic terms may be used to achieve selectivity of the faradaic component as well as exceptionally favorable faradaic-to-background-current ratios.

Another term whose influence needs to be carefully considered in FT voltammetry is R_u, which may modify both the faradaic and the nonfaradaic contributions to a voltammogram in a well-defined manner governed by Ohm's law. Significantly, this means that the second-order faradaic terms are very sensitive to the ohmic IR_u drop effect. Because the concentration of the electroactive species governs the faradaic component of I, this term also determines how sensitive the experimental data are to IR_u effects, as does the value of R_u itself. Consequently, for IR_u evaluation purposes, as well as mechanistic confirmation, experimental data should always be obtained at two or more concentrations. The common practice of deducing the contribution of IR_u and the mechanism on the basis of data obtained from a single concentration is fraught with danger.

A unified approach in voltammetry has been achieved by combining many of the strategies that have made FT-NMR such a powerful technique (*13*). Figures 2a and 2b illustrate the well-known NMR spectra that repre-

sent the transformation of experimental data from the time to the frequency domain. From a human perspective, the pattern in the frequency domain is remarkably easy to analyze relative to that in the time domain. For example, if rapid exchange processes are present, the modified pattern, in conjunction with modeling, improves understanding of the molecular dynamics in a far more intuitively obvious manner than does inspection of the time-domain data.

The power of presenting data in discrete packages of information derived directly from the FT algorithm applied to time-dependent data should not be underestimated. In FT-NMR, time-dependent data are rarely displayed anymore. Similarly, applying the FT approach in electrochemistry provides a visually useful power spectrum that separates individual frequency contributions (Figure 2d). Subsequent use of the inverse FT on each of these contributions generates even more powerful images (Figure 2e). We suggest that these forms of data presentation are more intuitively meaningful than the equivalent circuit approach, which is widely used in impedance spectroscopy. However, all forms of voltammetric data evaluation must be mathematically related, and the equivalent circuit form does have an undeniable mathematical elegance.

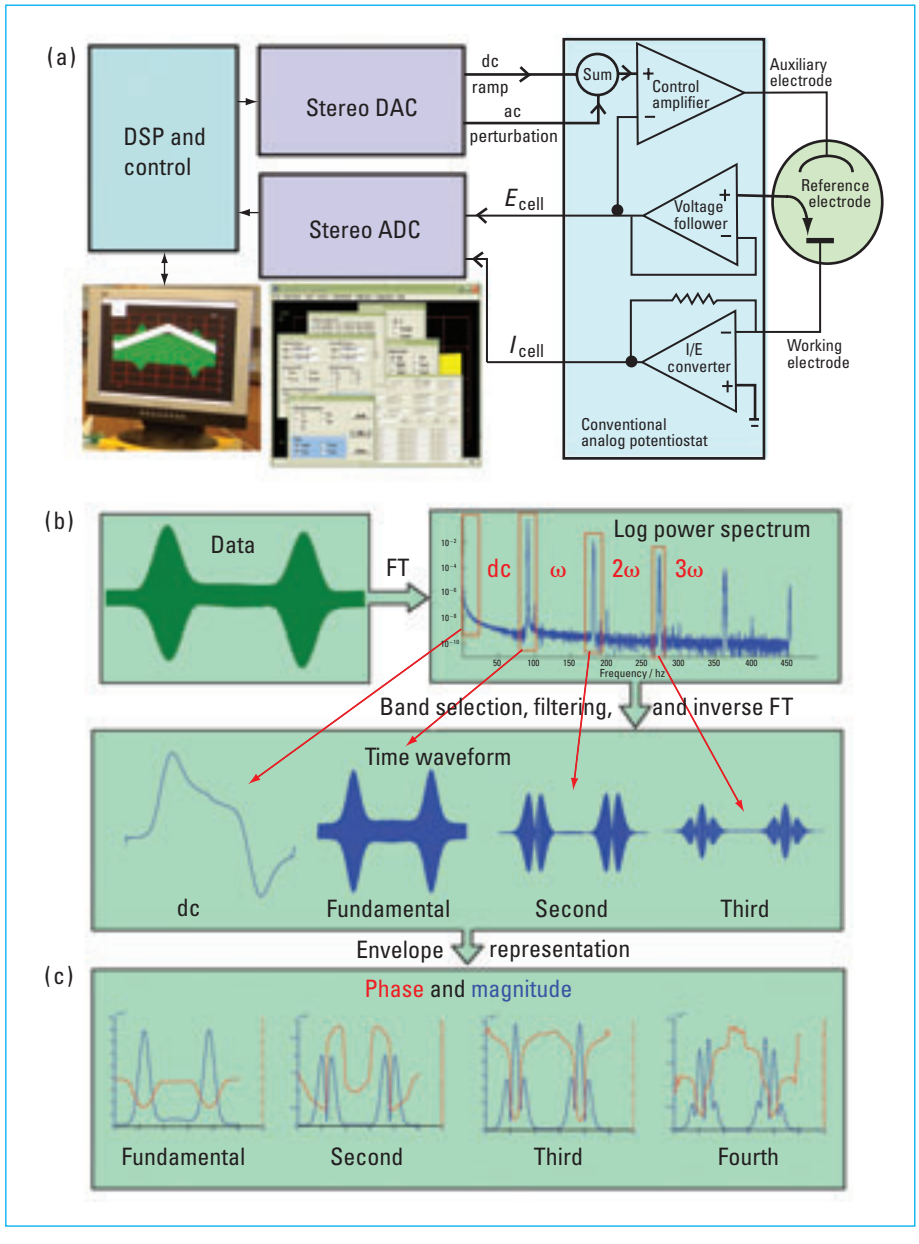

FIGURE 3. Schematics of (a) FT voltammetric instrumentation and (b, c) data processing methodology used in our laboratories.

Instrumentation

Figure 3a summarizes the key features in low-cost instrumentation needed to achieve a unified approach to FT voltammetry. A 2.5-GHz Pentium 4 desktop computer can be used for data analysis and instrument control. The other necessary hardware components are widely used in commercial stereo systems. The analog-to-digital converters (ADCs) and digital-to-analog converters (DACs) are ΔΣ-modulated devices that minimize the need for analog signal conditioning hardware and facilitate the production of a reliable, stable, and versatile system. Software compensates for the time delay introduced through the ADC and DAC devices (~33 samples each). Stereo hardware limits the upper sampling rate to ~40 kHz. This implies that the upper usable frequency is 20 kHz, because Nyquist's theorem requires the sampling rate to be at least twice the highest-frequency component of the signal being analyzed (*9*). For specialized applications requiring higher frequencies, more expensive and faster ADCs and DACs could be used.

The first requirement for a universal approach is a digital processing system that can generate a waveform containing both a highly linear dc ramp and designated combinations of sine waves of known frequency, amplitude, and phase; an 18-bit stereo DAC (Crystal Semiconductor Corp.) is ideal for this purpose. This DAC can produce a dc ramp with a potential range of ±3 V. The use of 18 or more bits produces voltage steps that are on the order of the instrument's thermal noise (~2 bits), thus generating a very low distortion analog dc ramp. The total response is dominated by the dc component and the fundamental harmonic. Thus, 18 or more bits are required to provide sufficient dynamic range to accurately measure all of the higher harmonic responses. When 14- or 16-bit devices are used, especially those without ΔΣ converters, the underlying dc component may produce unwanted frequency components in the FT and limit the

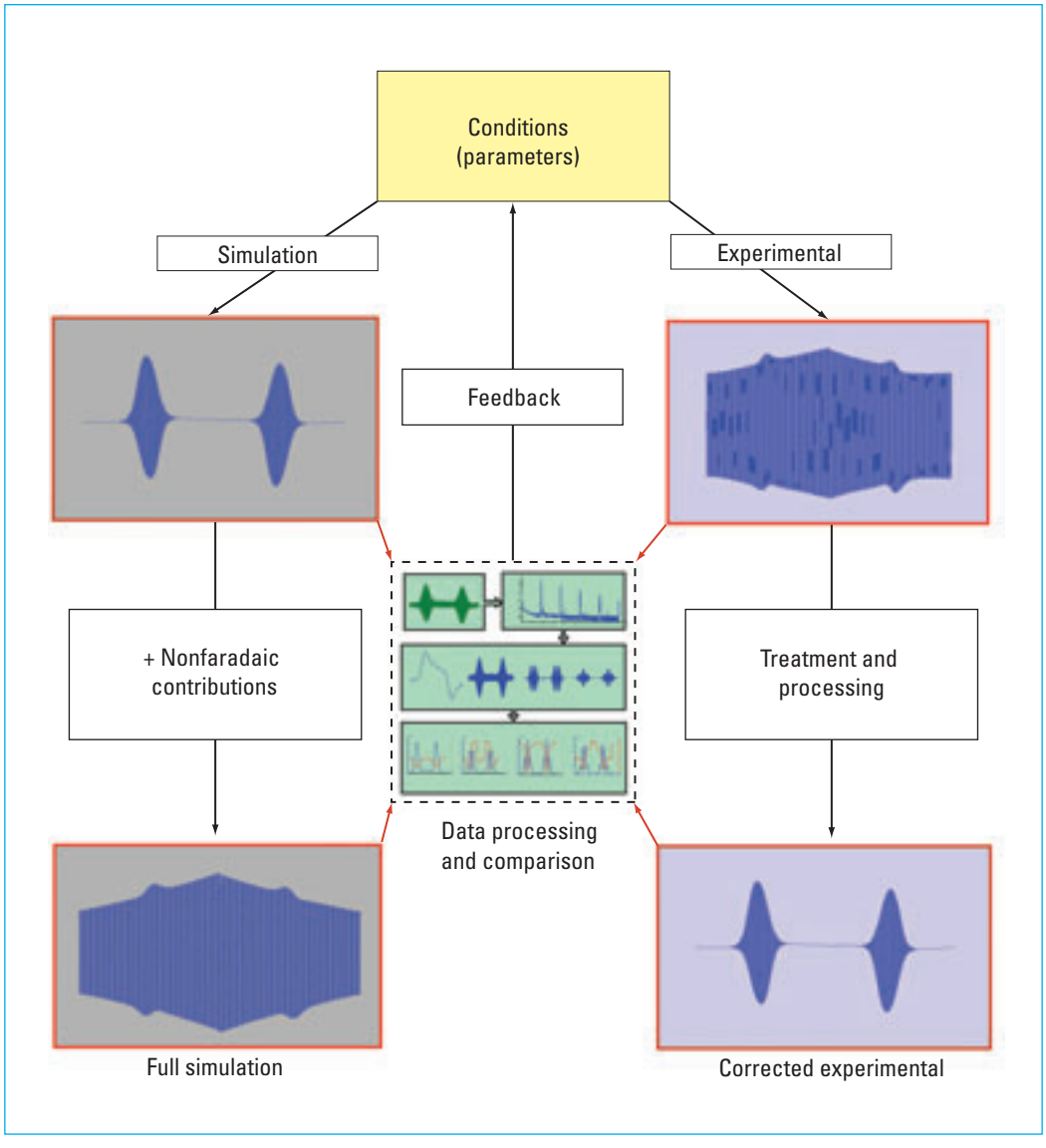

FIGURE 4. Schematic of a strategy for comparing experimental and simulated FT voltammetric responses.

accuracy of the harmonic analysis. In our instrument, dc scan rates up to 1000 V/s are available; at least one, but preferably many, cycles of the superimposed waveform should be applied.

A lookup-table digital signal processor (DSP) and control in Figure 3a stores a digital waveform, which is a highly accurate, 18-bit sine wave of amplitude ±300 mV; a Fourier series of sine waves (e.g., square wave); a selected combination of sine waves (impedance spectroscopy); or a user-defined waveform. In the case of a square wave, the operator may select any designated number of terms (k in Equation 4) in the Fourier series to achieve the required level of approximation to a true square wave. The initial 35 terms provide an extremely good approximation of this waveform and avoid a step function that complicates the analysis of a true square wave. In practice, simulations of the theory can use an exact replica of the waveform in the experiment, and only the number of terms in the Fourier series must be known. The digitally generated linear dc ramp and the operator-designated ac perturbation are converted to analog signals and summed (Figure 3a). This waveform, represented as $E_t = E_{dc} + E_{ac}$, is then fed to a conventional op-amp-based potentiostat with a rise time of ≤10 μs (*14*). The potentiostat controls a conventional working, reference-, and auxiliary-electrode cell configuration. Finally, the experiment is arranged so that exactly 2^n pairs (convenient for FT) of I–E data points are collected at a constant sampling rate and stored digitally; this is accomplished by an 18-bit stereo ADC preceded by a software-adjustable current amplifier (5 decade ranges covering 3 mA down to 30 nA full-scale). The data set is untreated at this stage except for a calibration procedure that ensures that any instrumentally introduced dc voltage offset or ac phase shifts are removed. After collection, the experimental data are interrogated by the software in the signal-processing section of the FT voltammetric instrumentation. In this case, an FT algorithm initially converts the time-domain data into the power spectrum (frequency domain) so that data are then displayed as packets of information.

Separation of all the components and their harmonics is achieved by selecting a frequency band that retains most of its energy and then zeroing the remaining portion of the power spectrum. Next, the inverse FT is applied to each selected component to generate the dc, fundamental, second-, third-, and higher-harmonic time-domain signals that provide highly informative patterns of behavior for the relevant mechanism. The pattern that emerges from the single sinusoidal waveform for a reversible process is shown in Figure 3b. The pattern of the power spectrum and the dc and harmonic components obtained after the inverse FT would differ significantly from that displayed in Figure 3b if a square wave or another form of multiple-sine-wave perturbation had been used. Other display formats include an envelope form rather than a full data set (Figure 3c) or impedance/admittance (real and imaginary) forms of presentation. We have also used commercially available software (MATLAB or

LabVIEW) to achieve the same data analysis outcomes. However, subsets of data may be analyzed that do not have to contain 2^n pairs of data points.

Simulations

Collecting experimental data is half the task in a voltammetric experiment; generating theoretical descriptions of all aspects of the electrode process is the other half. Simulations are progressively modified until an acceptable agreement with the experiment is achieved (*15*). dc Voltammetry is exceptionally popular because it produces voltammograms that can be intuitively understood. Commercially available simulation packages can accommodate a wide range of mechanisms. DigiSim is a popular simulation package that is extremely robust, versatile, and exceptionally user-friendly.

Fortunately, if a dc simulation of an electrode process is available, then an exactly analogous computational protocol can be used to simulate any form of FT voltammetry. This analogy applies to the treatment of faradaic (electron-transfer, coupled chemical reactions) and nonfaradaic (R_u, C_{dl}) components of the electrode process. In our preferred approach, the waveform used in the simulation is identical to that in the experiment. In this case, the simulations also generate outputs consisting of exactly 2^n $I(t)$–$E(t)$ data pairs. In this strategy, the simulated data may simply replace the experimental output in the analysis. That is, the instrumental data-processing methodology summarized in Figure 3b is used in an identical manner whether the 2^n pairs of data points are derived by experiment or by simulation. If commercially available FT software is used to evaluate experimental data, then the simulated data are still analyzed in an identical manner.

Although the simulations take more computer time than is the case with dc CV, the principles are the same. Consequently, tricks used to produce efficient simulations will be automatically advantageous in simulations of FT voltammetry. Also note that the computational power required for instrumental needs is more than enough for FT voltammetry simulations.

Simulation versus experiment

Two options are available for the final evaluation of the experiment (Figure 4). Raw data can be compared with those from a simulated model that takes into account the combined effects of the uncompensated resistance and faradaic and background currents. Alternatively, one can mathematically attempt to remove the contributions arising from R_u and background-current terms and compare them with simulations solely developed for the faradaic process. In any case, the protocol used is independent of whether the waveform is traditionally associated with ac, square-wave, staircase, or other voltammetry or impedance spectroscopy or is derived from an arbitrary periodic waveform.

The next level of development in FT voltammetry should focus on extensive exploitation of readily accessible patterns of behavior.

However, it cannot be emphasized too strongly that the relative sensitivities of each frequency component are solely determined by the nuances of the electron-transfer process, R_u, C_{dl}, and so forth. For example, in the single-large-amplitude-sine-wave experiment relevant to the reaction described by Equation 1, the dc component may provide an optimal initial estimate of the reversible potential; the fundamental harmonic provides an initial estimate of C_{dl}; and the second harmonic provides an initial estimate of R_u, the heterogeneous rate constant k_0, and the charge transfer coefficient α (*15*).

If a realistic mechanism has been identified, simulated and experimental dc data and all ac components should be in agreement within certain limits. If this is not the case, the simulation is varied until the required level of agreement is achieved. Ideally, all experimental and simulated data will be compared at a minimum of two different analyte concentrations to ensure that the IR_u, background, and electrode kinetic terms have been correctly analyzed. Often, it is not feasible to distinguish between the influence of two sets of parameters or distinguish between two different mechanisms on the basis of theory–experiment comparisons obtained from a single-scan-rate, single-concentration, dc experiment. Although the probability of obtaining a unique solution is markedly higher when FT forms of voltammetry are used, experiment-simulated comparisons over a range of frequencies, scan rates, and concentrations are always recommended (*15*). For example, a distinction between IR_u and slow electron-transfer kinetics can be readily made on the basis of the concentration dependence.

Exploiting patterns of behavior

The following examples illustrate the user-friendliness of FT voltammetry in terms of easily recognizing intuitively obvious patterns of behavior and achieving different levels of sensitivity in electron transfer and background processes in harmonic analysis.

Azurin. The dc and fundamental-harmonic data (Figures 5a and 5b) derived from a single-sine-wave experiment at a paraffin-impregnated graphite electrode barely enable the quasireversible surface-confined azurin faradaic process to be distinguished from the background current (*12*). In contrast, the second, third, and higher harmonics are almost devoid of background current (Figures 5c and 5d). It is obvious that for the azurin process, the dc and fundamental-harmonic components are the most convenient for quantifying the background process, whereas the second and higher harmonics emphasize and simplify the analysis of the faradaic component. When a square-wave perturbation is used, an entirely different pattern emerges (Figures 5e and 5f; *16*). In this case, the dc component and all odd harmonics are very sensitive to the background, but the even harmonics are almost purely faradaic. Interestingly, a novel form of kinetic selectivity also is ex-

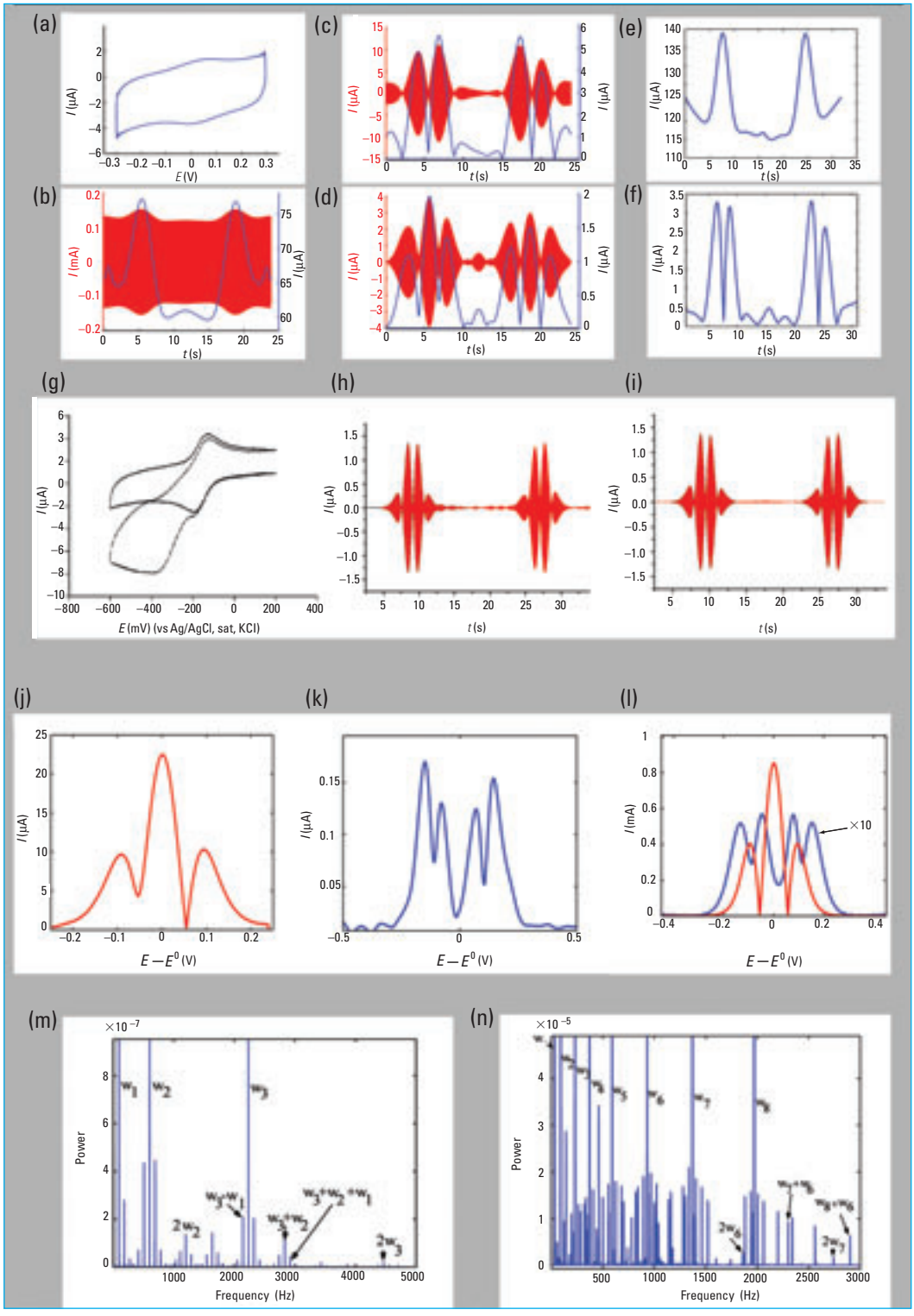

FIGURE 5. Examples of patterns of behavior observed in FT voltammetry.

Surface-confined azurin process: (a) dc; time (red) and envelope (blue) forms of representation of the (b) fundamental and (c, d) higher harmonics derived from a single-sine-wave experiment at a paraffin-impregnated graphite electrode. (Adapted from Ref. 12.) (e) Odd and (f) even harmonics obtained from a 70-term Fourier series square-wave (Equation 6) voltammogram. (g) dc and (h, i) fourth-harmonic FT single-sine-waveform cyclic voltammograms for reduction of 0.2 mM $[Ru(NH_3)_6]^{3+}$ in aqueous 0.5-M KCl solution at a glassy carbon electrode in the (g ----, h) presence and (g —, i) absence of O_2. (Adapted from Ref. 16.) Illustration of IR_u effect in the third harmonic of the reversible oxidation of ferrocene in dichloromethane (0.1 M Bu_4NPF_6) at a platinum electrode at (j) 0.12 mM and (k) 1.0 mM. (Adapted from Ref. 15.) (l) Simulations for 1.0 mM with R_u = 3400 (—) and 0 Ω (—). Power spectra from (m) 3-component (90.6, 598.43, and 2231.0 Hz) and (n) 8-component (35.17, 90.0, 230.07, 370.14, 590.09, 930.43, 1370.31, and 1970.53 Hz) sinusoidal waveforms for oxidation of 0.1 mM ferrocene at a platinum electrode in acetonitrile (0.1 M Bu_4NPF_6).

hibited for the square-wave technique—the even harmonic component is absent for a fully reversible process without an IR_u drop (*16*, *17*). Again, this is a consequence of the nonlinearity of the faradaic process.

$[Ru(NH_3)_6]^{3+}$. In the dc component of the reversible reduction of $[Ru(NH_3)_6]^{3+}$ in the presence of the irreversible reduction of oxygen, both processes are unresolved (Figure 5g; *18*). In contrast, in the fourth harmonic of a single-sine-wave experiment, only the reversible $[Ru(NH_3)_6]^{3+/2+}$ process is detected (Figures 5h and 5i). Thus, kinetic selection (reversible vs irreversible processes in this case) is possible via harmonic analysis. However, some combinations of sine waves may produce different patterns of behavior that discriminate against a reversible process; for example, the square-wave series leads to no response for the even harmonics but a measurable response for a quasireversible process (*16*, *17*, *19*).

Ferrocene. In the reversible oxidation of 0.12 mM ferrocene in highly resistive dichloromethane, the third harmonic for a single-sine-wave experiment generates the usual 3-peak response (Figure 5j; *15*). However, 4 peaks are detected at 1 mM (Figure 5k). Simulations demonstrate that the presence of 3400 Ω of uncompensated resistance has a large influence at 1 mM but almost negligible influence at 0.1 mM (Figure 5l).

$[Fe(CN)_6]^{3-}$. In the quasireversible reduction of

$[Fe(CN)_6]^{3-}$, very rich patterns of behavior can be seen after 3 and 8 nonharmonically related sine waves are applied and the data are analyzed in the frequency domain (Figures 5m and 5n; *16*). The significantly different power spectra obtained with other forms of FT voltammetry highlight the fact that the relative sensitivity of the faradaic and nonfaradaic terms is technique- and harmonic-dependent.

These examples are restricted to simple electron-transfer studies at stationary macrodisc electrodes. Electrode processes that contain other forms of mass transport (e.g., microdisc electrodes [*20*], hydrodynamic control, migration) and/or chemical reactions coupled to electron-transfer processes also are assisted by our integrated approach to FT voltammetric analysis.

Overview

The integrated approach to voltammetry and impedance spectroscopy advocated in this article emanates from a vast knowledge base (*21*, *22*). A summary of the evolution of the convergence of ac voltammetric and impedance methodologies has recently been presented by Roy et al. (*23*). However, the current availability of high-speed, low-cost instrumentation with vast amounts of memory and computing power, combined with equivalently impressive developments in simulation, removes the need to restrict studies to linear, small-amplitude regions for data analysis. The full power of information-rich, nonlinear harmonic analysis can now be applied. Because a dc component is available in the FT voltammetric approach, the elegance and simplicity of the dc methodologies are retained.

The next level of development in FT voltammetry should focus on extensive exploitation of readily accessible patterns of behavior. To date, we have utilized this modus operandi in a heuristic manner. However, the power of pattern recognition in a mathematical context should produce computer-based, intelligently generated, arbitrary waveforms that lead directly to the optimal objective of the experiment (*24*). In an analytical context, the objective may be the maximum faradaic-to-background-current ratio achievable for trace concentration determinations. In a fundamental study, the key objective may be kinetic resolution of overlapping processes or detection of frequency dispersion in the redox chemistry of surface-confined processes (*12*). The best way to achieve these goals may not be ac, square-wave, pulse, or impedance spectroscopy waveforms—it may be an arbitrary waveform that has yet to be used in a voltammetric experiment.

Financial support from the Australian Research Council and extensive discussions with S. W. Feldberg, D. J. Gavaghan, K. Gillow, K. B. Oldham, and A. A. Sher on the theory of FT voltammetry are gratefully acknowledged.

Alan M. Bond is a professor and Noel W. Duffy, Si-Xuan Guo, and Jie Zhang are postdoctoral research fellows at Monash University (Australia). Bond's research concentrates on theoretical, instrumental, and applied aspects of electroanalytical chemistry. Duffy is interested in developing electrochemical and photoelectrochemical techniques. Guo's research interests include ac voltammetry, protein film voltammetry, inorganic electrochemistry, and chemically modified electrodes. Zhang's research focuses on ultramicroelectrode techniques, liquid/liquid interfaces, Langmuir trough techniques, biosensors, ionic liquids, and numerical simulations. Darrell Elton is a lecturer in electrical engineering at La Trobe University (Australia). His research focuses on instrumental and computational aspects of electrochemistry. Address correspondence about this article to Bond at alan.bond@sci.monash.edu.au.

References

(1) Rieger, P. H. *Electrochemistry*, 2nd ed.; Chapman & Hall: New York, 1994.
(2) Bond, A. M. *Broadening Electrochemical Horizons*; Oxford University Press: Oxford, UK, 2002.
(3) Bard, A. J.; Faulkner, L. R. *Electrochemical Methods*, 2nd ed.; Wiley & Sons: New York, 2001.
(4) Gosser, D. K. J. *Cyclic Voltammetry: Simulation and Analysis of Reaction Mechanisms*; VCH Publishers: New York, 1993.
(5) Macdonald, J. R. *Impedance Spectroscopy: Emphasizing Solid Materials and Systems*; Wiley Interscience: NJ, 1987.
(6) Scully, J. R.; Silverman, D. C.; Kendig, M. W. *Electrochemical Impedance: Analysis and Interpretation*; American Society for Testing and Materials: West Conshohocken, PA, 1993.
(7) Bond, A. M. *Modern Polorogaphic Methods in Analytical Chemistry*; Marcel Dekker: New York, 1980.
(8) Smith, D. E. In *Electroanalytical Chemistry*; Bard, A. J., Ed.; Marcel Dekker: New York, 1966; Vol. 1, pp 1–148.
(9) Sluyters-Rehbach, M.; Sluyters, J. H. In *Electroanalytical Chemistry*; Bard, A. J., Ed.; Marcel Dekker: New York, 1970; Vol. 4, pp 1–121.
(10) Osteryoung, J.; O'Dea, J. J. In *Electroanalytical Chemistry*; Bard, A. J., Ed.; Marcel Dekker: New York, 1986; Vol. 14, pp 209–303.
(11) Spanier, J.; Oldham, K. B. *An Altas of Functions*; Hemisphere: New York, 1987.
(12) Guo, S.-X.; et al. *Anal. Chem.* **2004**, *76*, 166–177.
(13) Roberts, J. D. *ABC's of FT-NMR*, 1st ed.; University Science Books: Sausalito, CA, 2000.
(14) Kissinger, P. T. In *Introduction to Analog Instrumentation in Laboratory Techniques in Electroanalytical Chemistry*; Kissinger, P. T., Heineman, W. R., Eds.; Marcel Dekker: New York, 1984; pp 163–192.
(15) Sher, A. A.; et al. *Anal. Chem.* **2004**, *76*, 6214–6228.
(16) Zhang, J.; et al. *J. Phys. Chem.*, in press.
(17) Sher, A. A.; et al. *Electroanalysis*, in press.
(18) Zhang, J.; et al. *Anal. Chem.* **2004**, *76*, 3619–3629.
(19) Rosvall, S. J. M.; Sharp, M.; Bond, A. M. *J. Electroanal. Chem.* **2003**, *546*, 51–58.
(20) Gavaghan, D. J.; Elton, D. M; Bond, A. M. *Collect. Czech. Chem. Commun.* **2001**, *66*, 255–275.
(21) Smith, D. E. *Anal. Chem.* **1976**, *48*, 221 A–240 A.
(22) Park, S.-M.; Yoo, J.-S. *Anal. Chem.* **2003**, *75*, 455 A–461 A.
(23) Garland, J. E.; Pettit, C. M.; Roy, D. *Electrochim. Acta* **2004**, *49*, 2623–2635.
(24) Neapolitan, R. E. *Learning Bayesian Networks*; Pearson Prentice Hall: Upper Saddle River, NJ, 2004.